JOURNAL OF AIRCRAFT
Vol. 35, No. 2, March–April 1998

Aeroelastic Computations on Wing–Body–Control Configurations on Parallel Computers

Chansup Byun* and Guru P. Guruswamy†
NASA Ames Research Center, Moffett Field, California 94035-1000

A multizonal capability for aeroelastic computation of complex geometries has been implemented in ENSAERO, an aeroelastic analysis code with Euler/Navier–Stokes flow solver, on the IBM SP2 parallel computer. The discipline parallelization is achieved by distributing the fluid, structure, and control domains onto different groups of computational nodes. The fluid domain is further parallelized based on the multizonal method. The coupling between the fluids and structures is obtained by exchanging the interface boundary data at every iteration by using the explicit message passing interface standard library. The performance of the current implementation shows that about 12 computational nodes of the SP2 computer are equivalent to the speed of a single C90 processor. For demonstration purposes, static aeroelastic computations coupled with control surfaces are made for an arrow wing–body–control configuration in the transonic flow regime. Computed pressure coefficients for a rigid configuration were compared with the wind-tunnel experiment. The two results show good agreement. Steady aeroelastic simulations are made with and without control surface deflections. The static aeroelastic simulations show that the effect of flexibility is significant on aerodynamic coefficients. It is noted that the flexible wing lowered the sectional lifts compared to the rigid wing. This procedure can be utilized for the fast computational solution of large-scale wind-tunnel models and real configurations that inevitably deform under aerodynamic loads.

Introduction

ACCURATE prediction of aeroelastic loads is necessary for the design of large flexible aircraft. Uncertainties in the characteristics of loads may result in an improper accounting for aeroelastic effects, leading to understrength or overweight designs and unacceptable fatigue life. Moreover, correct prediction of loads and the resultant structural deformations are also essential to the determination of the aircraft stability and control characteristics. Because the experimental evaluation would involve considerable cost and the risk of structural damage in a wind tunnel, it is necessary to implement the investigation through theoretical analyses.

Critical design conditions occur in the transonic regime by mixed flow, embedded shocks, separation, and vortical flow. Furthermore, aircraft are often subject to aeroelastic oscillation because of flow unsteadiness. In this unsteady aerodynamic environment, many modern aircraft rely heavily on active controls for safe and steady flight operation.

For the numerical simulation of flow in complex geometries, the multizonal method is widely employed. This method is based on domain decomposition techniques, with the flow domain being partitioned into a number of subdomains (zones). Within each subdomain, the flow equations are solved in an independent manner, with the global nature of the flow being accounted for by the periodic exchange of boundary information between neighboring zones. Therefore, for complex geometries it is necessary to integrate the multizonal method for fluids into aeroelastic computations.

Received July 17, 1996; revision received July 14, 1997; accepted for publication Sept. 3, 1997.

*Senior Research Scientist, Applied Computational Aerodynamics Branch, MCAT Institute. Member AIAA.

†Research Scientist, Applied Computational Aerodynamics Branch. Associate Fellow AIAA.

The present investigation is initiated in conjunction with the ENSAERO code, which is capable of computing aeroelastic responses by simultaneously integrating the Euler/Navier–Stokes equations and the modal or the finite element structural equations of motion using aeroelastically adaptive dynamic grids.[1–5] The patched zonal grid technology based on the work in Ref. 6 has been implemented for the flow computations of complex geometries. The code has been applied to transonic flows from small to moderately large angles of attack for fighter wings undergoing unsteady motions. The code was extended to simulate unsteady flows over rigid wing and wing–body configurations with an oscillating trailing-edge flap by using either single or patched multizonal grids. The code has been parallelized and demonstrated aeroelastic computations for wing and wing–body configurations[7] on the Intel iPSC/860 parallel computer. In this parallelized version, the computational grid for the fluids is assumed to be a single zone for aeroelastic computations. However, in this research, the code has been parallelized based on the multizonal method to handle complex geometries on distributed memory, multiple-instruction, multiple-data (MIMD) type parallel computers. The data communication between computational nodes is achieved by using the MPIRUN (Ref. 8) library. Because the MPIRUN library is based on the message passing interface (MPI) standard (Ref. 9), the parallel version will run without modification on any MIMD-type computer supporting the MPI standard. For demonstration purposes, the IBM SP2 computer is selected.

This paper presents the results of steady aeroelastic and unsteady Navier–Stokes simulations of transonic flows over a flexible arrow wing–body configuration with an oscillating control surface. An arrow–wing configuration has been studied as a design concept for supersonic civil transport.[10] Because of the highly swept thin wing, it is known that transonic flutter is a design problem on this configuration.[11] Computations have been made with and without control surface deflections. Computed pressure coefficients for a rigid configuration have been compared with the wind-tunnel experiment.[10] Steady aeroelastic simulations are made without and with control surface deflections. The static aeroelastic simulations show

that the effect of flexibility is significant on aerodynamic coefficients. It is noted that the flexible wing significantly reduced the sectional lifts compared to the rigid wing. This computational procedure can be used for the fast computational solution of large-scale wind-tunnel models and real configurations that inevitably deform under aerodynamic loads.

Numerical Methods

The governing aeroelastic equations of motion can be written as

$$[M]\{\ddot{q}\} + [C]\{\dot{q}\} + [K]\{q\} = \{Z\} \tag{1}$$

where $[M]$, $[C]$, and $[K]$ are the global mass, damping, and stiffness matrices of structures, respectively. $\{Z\}$ is the aerodynamic force vector corresponding to the displacement vector $\{q\}$. These quantities can be expressed as modal or finite element equations, depending on the method used to obtain the structural dynamic responses. One of the main efforts is computing the global force vector $\{Z\}$ of Eq. (1). In this work, for a given time t, $\{Z\}$ is computed by solving the Navier–Stokes equations.

The nondimensionalized Reynolds-averaged thin-layer Navier–Stokes equations are used for the fluid domain in this study. The viscosity coefficient is computed as the sum of the laminar and turbulent viscosity coefficients, where the laminar viscosity is taken from the freestream laminar viscosity, assumed to be constant for transonic flows. As an option, Sutherland's law can be used to calculate the laminar viscosity. The turbulent viscosity is evaluated by the Baldwin–Lomax algebraic eddy–viscosity model.[12] Because the flowfield considered in this paper contains leading-edge separation, a modification to the turbulence model originally developed for crossflow-type separation[13] is applied.

Several numerical schemes have been developed to solve the Navier–Stokes equations. The present code has two different schemes for the inviscid terms: 1) the central difference and 2) streamwise upwind schemes. A second-order central difference evaluation is applied to the viscous terms. An implicit method is used for the time integration because it is more suitable for expensive unsteady viscous calculations. A complete description of the algorithm can be found in Ref. 2.

In this study, the response of the structure under steady and unsteady dynamic loads is obtained by solving the modal equations of motion. For the aeroelastic simulation of the arrow wing–body configuration, only the wing portion is allowed to be flexible for this study. In addition, in this study, the control surface movement is obtained by prescribing the maximum angle of rotation and the frequency of oscillation.

For static aeroelasticity analysis, because $\ddot{q} = \dot{q} = 0$, a primary static option uses

$$[K]\{q\} = \{Z\} \tag{2}$$

in conjunction with the steady flow computation using a locally varying time step. However, this often causes significant numerical oscillations because there is no damping in the system.[14] These oscillations are initiated by numerical transients. To obtain a smooth numerical transition, a pseudodynamic method, which adds significant damping to the system, is used. The damping coefficients are set so that all transient modes damp out quickly. The damping matrix is computed using the relation

$$[D] = \alpha[M] + \beta[K] \tag{3}$$

where α and β are constants to be determined from two assumed damping coefficients that correspond to two selected modes of vibration. More details about the computation of $[D]$ can be found in Chap. 9 of Ref. 15. For the computations presented in this paper, the two damping coefficients of the first two modes are selected as 0.6 and 0.8, respectively. These values for α and β give an artificial shock absorber for structural oscillations caused by flow transients.

In the present domain decomposition approach, coupling between the fluid and structure domains is achieved by exchanging boundary data, such as aerodynamic pressures and structural deflections, at each time step. An analytical moving grid technique has been successfully used to deform the aerodynamic grid according to the structural deflections at the end of every time step.[3,7,16] A shearing method is used to deform the volume grid because the surface grid deformation following the structural deformation considered in this work is small.

Parallel Implementations

The domain decomposition approach used in ENSAERO is suitable for parallelization. The discipline parallelization is achieved by distributing the fluid, structure, and control domains onto different groups of computational nodes. Only a single computational node is assigned to the structure and control groups because the computational load is relatively small for the structure and control. The fluid domain is further parallelized based on the multizonal method. This is considered as the coarse-grain parallelization. Several computational nodes are assigned to the fluid domain. Each computational node solves the flow equations for each zone. The zonal boundaries are then updated by exchanging boundary information between neighboring zones.

The communication required for the parallelization is accomplished by using MPIRUN (Ref. 8), a utility developed by the National Academy of Sciences parallel systems group at NASA Ames Research Center. MPIRUN flexibly defines a group of computational nodes and enables communicating data within a group or between groups. MPIRUN is based on the MPI standard.[9]

The serial version of ENSAERO treats each zone of the grids sequentially, while the other zones reside in a secondary storage device (SSD) such as on a Cray C90. The current implementation exploits the functional parallelism among multiple zones of patched grids. As a result, all zones are computed concurrently.

The interpolation and communication of the zonal boundary data is done concurrently, through a loosely synchronous approach. At the end of each step, computational nodes holding zonal boundary surfaces send the interpolated flowfield data to the appropriate computational nodes of the other zones. Each computational node proceeds to the computations of the next step of the flow solver as soon as its zonal communication phase is completed. Because this implementation is based on the multizonal method, there will be significant load imbalances between computational nodes unless the grid size of each zone is close to each other. This load imbalance can be avoided by designing the size of each zonal grid as close to each other as possible. The load balancing can also be achieved by decomposing each zonal grid into smaller subgrids in conjunction with the parallelization of the flow solver. However, this is not considered here because it is beyond the scope of this paper.

To couple the fluid, structure, and control domains, communication between domains is also accomplished through an interface at the end of each time step. The aerodynamic loads are converted into the structural loads through the fluid–structural interface.[16] Also, structural deformation is passed to the fluid domain through the interface. Then, the surface grid is deformed according to the structural deformation. In addition, control surface deflection is superimposed on the deformed surface grid.

Model Geometry and Grid

An H–H topology grid is used for a wing–body configuration with a control surface, which is a trailing-edge flap in this case. This topology is chosen to easily align grid lines to the control surface. The ICEM DDN CAD software system[17]

was used to generate the surface grid. From the surface grid, the volume grid was generated by using the HYPGEN code.[18] Although the experimental model[10] has two flaps at both the leading and trailing edges, only the outboard flap at the trailing edge is considered in this paper.

Figure 1 shows the geometry of the wind-tunnel model. The configuration has a thin, low aspect ratio, highly swept wing mounted below the centerline of a slender body. The wing is flat with a rounded leading edge. Note that the exact wing tip definition was not available, and so the tip thickness was decreased to zero across three grid points.

Figure 2 shows the overview of the surface grid for the full-span configuration (the grid lines on the wing are shown for every other line). The reference length is taken from the mean aerodynamic chord, and the origin of the coordinates is set at the nose of the body. The body is extended to the downstream boundary. The half-span grid used for symmetric cases consists of 110 points in the streamwise direction, 116 points in the spanwise direction, and 40 points normal to the body surface, for a total of 510,400 points. Bilateral symmetry is imposed in the $x-z$ plane at $y = 0$ (the center of body). In the following computations, the grid is further divided into the upper and lower grids at the wing and the H-topology cut condition is provided through a zonal interface. Flow variables at the zonal interfaces were updated as soon as the adjoining zones were computed. The same procedure can be applied to unsteady calculations at every time step.

For the parallel computation, the original grid was split into eight patched zonal grids to be distributed on eight nodes of the SP2 computer as shown in Fig. 2. Each grid has the same amount of grid points by dividing uniformly in longitudinal and spanwise directions.

To treat the control surface movement without introducing additional zones, a small gap is introduced at the end of the control surface. This region is used to shear the grid when the control surface oscillates. The dynamic grid around a deflected control surface was obtained by shearing every grid line normal to the control surface with the local deflection, Δx and Δz. Grid deformation caused by structural deflections is also treated in a similar fashion.

In the experiment, a transition strip was placed at the 15% chord. However, the report did not show significant differences in comparisons of force measurement with and without the strip in the transonic regime.[9] In addition, the effect of the strip on the separation at the leading edge was not very clear. Thus, in the computation, a fully turbulent flow is assumed.

The grid lines on the body surface collapse to a point at the nose and extend upstream as a singular axis. The flow variables on the singular axis are given by taking an average from the surrounding grid points. When a computation starts im-

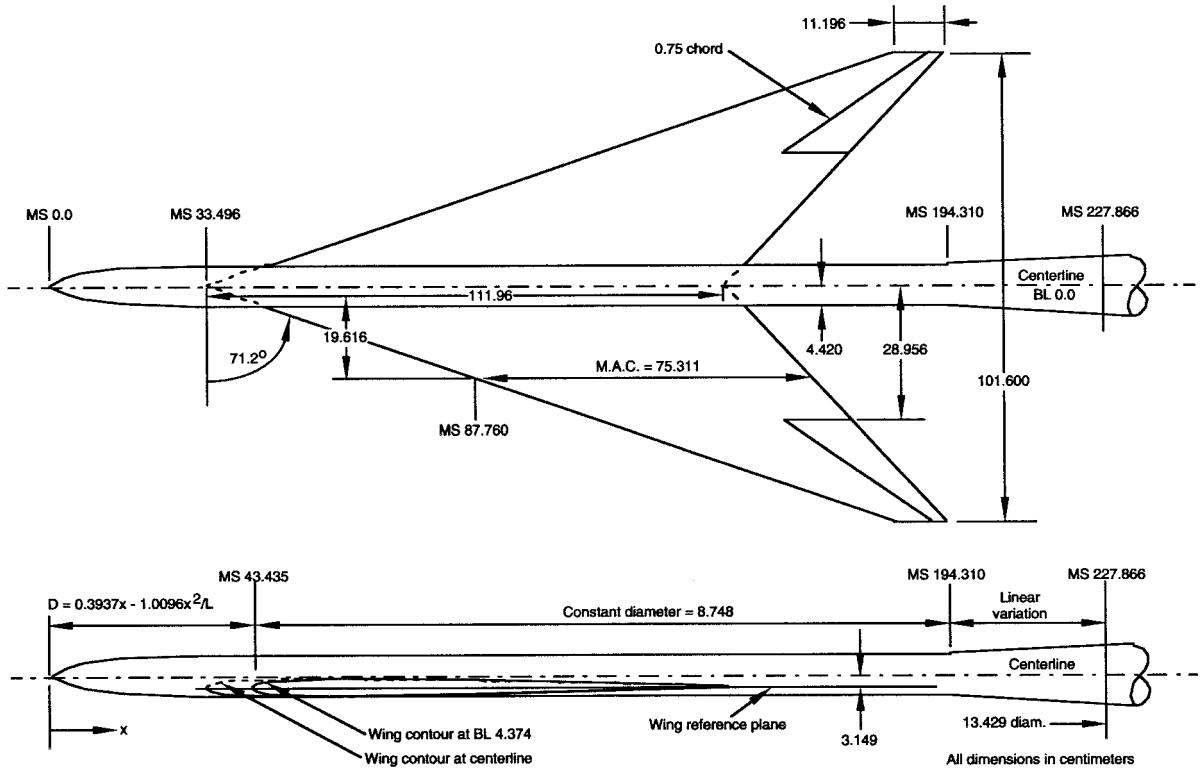

Fig. 1 Wind-tunnel model geometry of an arrow wing–body configuration.

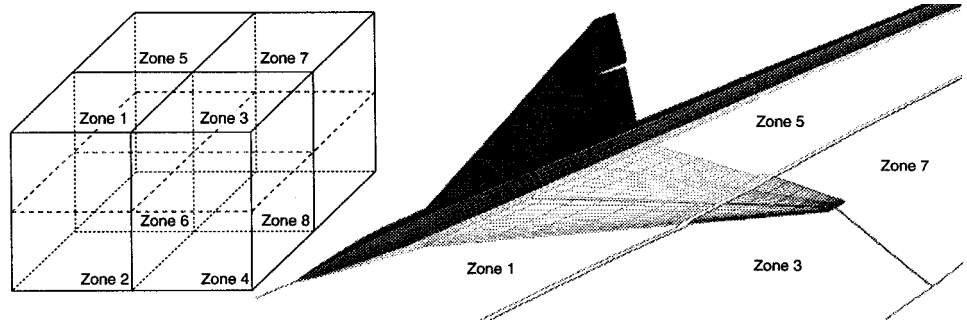

Fig. 2 Overview of the upper surface grid with a deformed control surface and the grid partition for eight zones.

pulsively from the freestream condition, the upwind method is not dissipative enough to damp the initial disturbances along the axis. The central difference option of the code was used to overcome this initial transient period. Because the upwind solution gave a crisper vortex structure for steady state, the upwind option was used for the rest of the calculations.

Results

Steady Flap Deflection

Figure 3 shows the steady pressures compared with the experiment at the 20, 50, and 80% semispanwise sections for the half-span configuration. The 80% section is located in the midspan of the control surface. The flow conditions consist of a Mach number $M_\infty = 0.85$, an angle of attack $\alpha = 7.93$ deg, a flap deflection $\delta = 0$ deg, and a Reynolds number $Re_{\bar{c}} = 9.5 \times 10^6$, based on the mean aerodynamic chord. Suction observed near the trailing edge at the 80% section corresponds to the leading-edge vortex. There is a minor discrepancy between the computation and the experiment because of the difference in the location of the leading-edge vortex. The computation predicts the vortex at a slightly more inboard location than the experiment. Possible sources of this difference are the effects of the transition strip and the wall of the wind

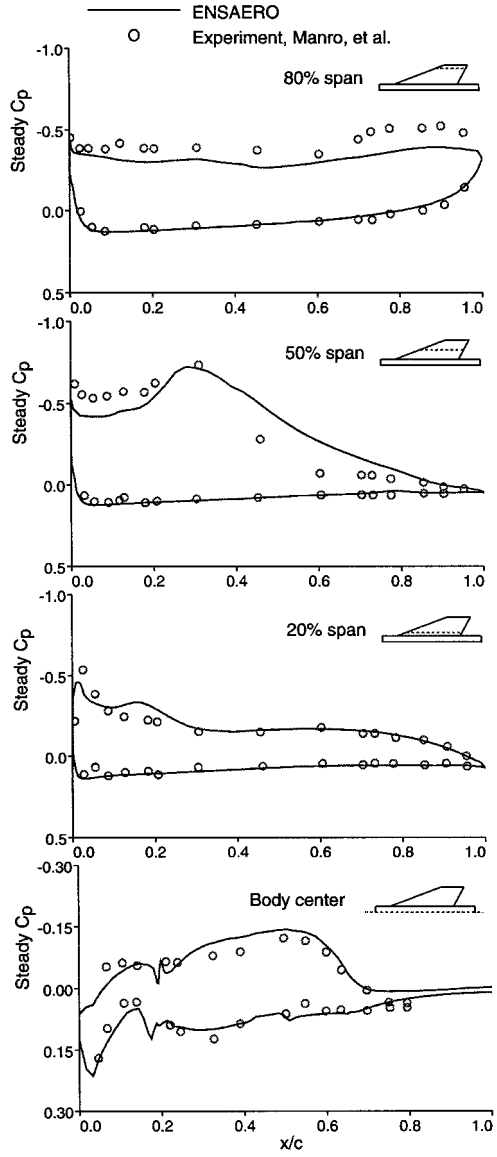

Fig. 3 Comparison of computed steady pressures with experiment; no flap deflection.

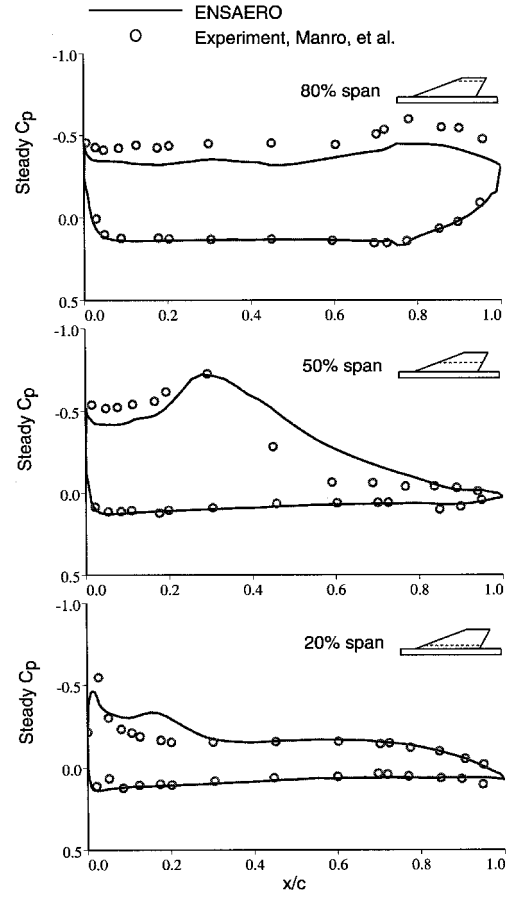

Fig. 4 Comparison of computed steady pressures with experiment; 8.3-deg flap-down deflection.

tunnel. No data corrections were applied to either the computed or measured data. Overall, the computed result shows good agreement with the experiment. The pressure distributions on the body center also show good agreement as shown in Fig. 3.

The corresponding result at the same flow condition with the flap deflected down by 8.3 deg is shown in Fig. 4. The effect of the flap deflection is apparent at the 80% spanwise section, although no streamwise separation is found on the flap surface. The kinks in the pressure profiles at the 75% chord correspond to the flap hinge. At the 50% spanwise section, the effect of the flap deflection is only found near the trailing edge. The effect is not noticeable at the 20% section. The computed pressure profiles capture the flow features well. The effect of the flap deflection is very small on the body and, thus, the pressure distributions are not shown here.

Unsteady Flow with Flap Motion

For the rigid wing–body–control configuration, unsteady flow simulation at the previous flow condition was performed by oscillating the flap surface at the maximum deflection of 8.3 deg. The flap oscillates at a reduced frequency of 0.6 (approximately 15 Hz). Figure 5 shows the instantaneous surface pressure distributions at the maximum flap down and up positions. The pressure distributions show that the largest difference occurred at the 80% section, which is the midsection of the flap, as expected. The effect of flap deflection appears only in a small region near the trailing edge at 50% section, and no effect is noticeable at the 20% section.

The overall surface pressure distribution is presented in Fig. 6. This result is obtained from the rigid unsteady flow–control simulation when the flap reached at 8.3-deg flap-up position. The particle traces clearly show the leading-edge vortex.

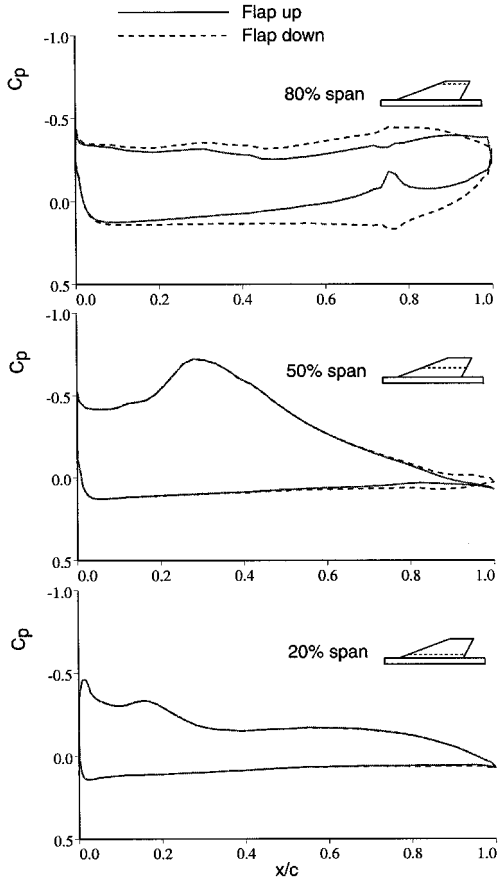

Fig. 5 Comparison of instantaneous pressures from a rigid unsteady flow–control simulation.

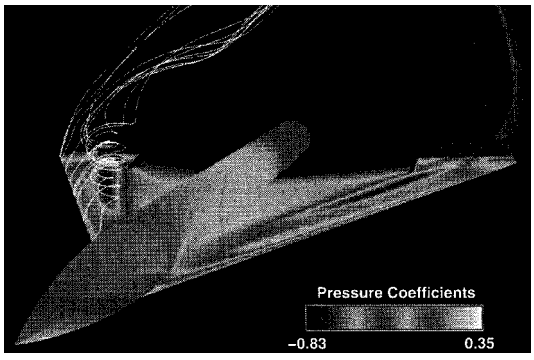

Fig. 6 Overall surface pressure distribution at 8.3-deg flap-up position.

Static Aeroelastic Computation

For the flexible wing–body–control configuration, first the static equilibrium position of the wing is obtained by performing static aeroelastic analysis without deforming the flap surface.

In this study, only the wing structure is allowed to be flexible, to separate the effect of body flexibility. The wing is modeled as a flat plate to generate the modal properties such as mode shapes and modal mass and stiffness matrices. The actual wind-tunnel model was too stiff to show the effect of flexibility, which apparently exists in the actual airplane. Thus, to demonstrate the effect of flexibility, the flexible wing was modeled as a flat steel plate with thickness of 0.1 in.

The coupled fluid–structure analysis has been iterated until the converged solutions for both domains are obtained. The convergence was monitored by the wing tip displacement. As the solution converges, the tip displacement also reaches an equilibrium state. At the equilibrium state, the steady pressure distributions at various span sections are compared with those from the rigid configuration. The results are shown in Fig. 7. As shown in Fig. 7, the flexible configuration causes significant changes in pressure distributions for all stations, including the body section, which is kept rigid during the simulation. It is noted that the sectional lifts at all sections are significantly reduced because of the flexibility effect of the wing structure.

The sectional twist variations because of the flexibility of the wing are presented in Fig. 8. As one approaches the wing tip, the deflection of the wing is increased because of structural bending, as expected. In addition, because the wing is highly swept, the trailing edge is deflected more than the leading edge, which causes a decrease in the local angle of attack.

The effects of flap deflection on static aeroelastic simulation are shown in Figs. 9 and 10. The sectional pressure distributions are compared at 50 and 80% sections in Fig. 9. As shown in Fig. 9, the effect of flap deflection is significant at the 80% section, where the flap is located. However, the effect rapidly diminishes away from the flap and is shown to be negligible at the 50% section. The flap-down configuration causes an increase in the sectional lift, whereas the flap-up configuration decreases the sectional lifts as compared to the one without flap deflection.

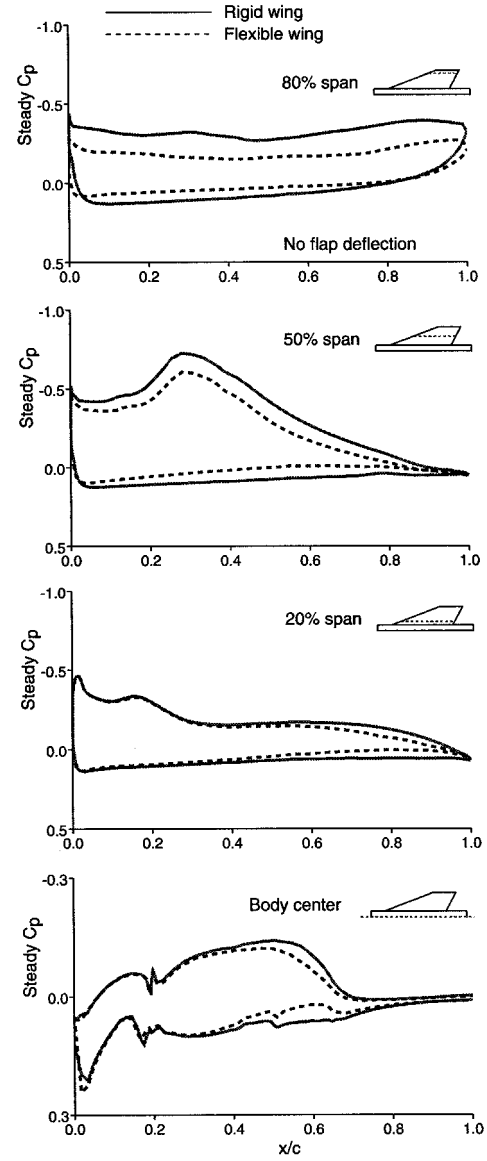

Fig. 7 Change of steady pressure distribution because of the flexibility of the wing structure: no flap deflection.

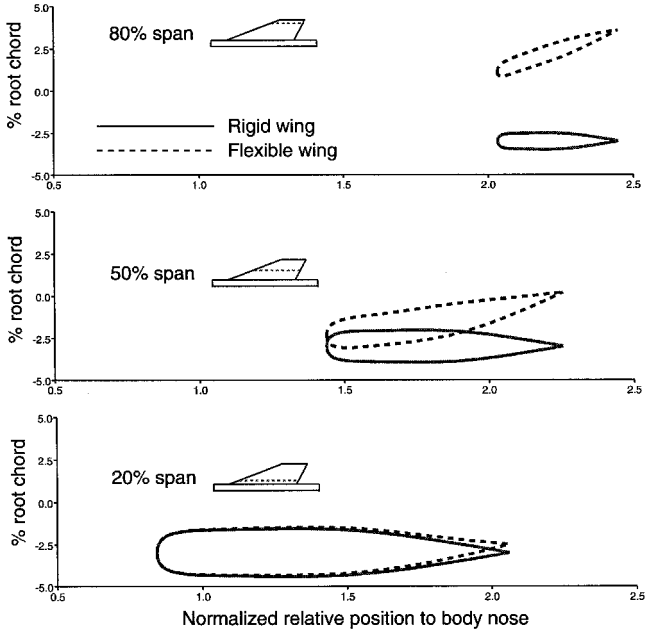

Fig. 8 Sectional twist variations for flexible wing configuration: no flap deflection.

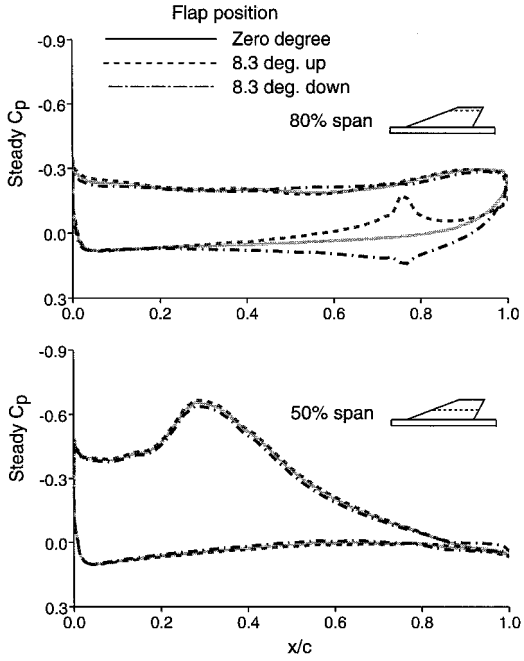

Fig. 9 Effect of flap deflection on sectional pressure distribution for a flexible wing structure.

It is observed that the largest deformation of the wing resulted from the flap-down configuration, as shown in Fig. 10. This is an expected result because the flap-down configuration caused larger sectional lift at the 80% section than the other configurations. At the 50% section, flap deflection causes slight changes in wing twist, which bring changes in local angle of attack, while bending displacements caused by flap deflection are negligible at this section. However, the effect on both bending and twisting displacements caused by flap deflection are clearly noticeable at the 80% section.

Performance

Preliminary data for performance measurement are shown in Fig. 11. This is obtained after porting the vectorized version of the code running on the Cray computer to the IBM SP2

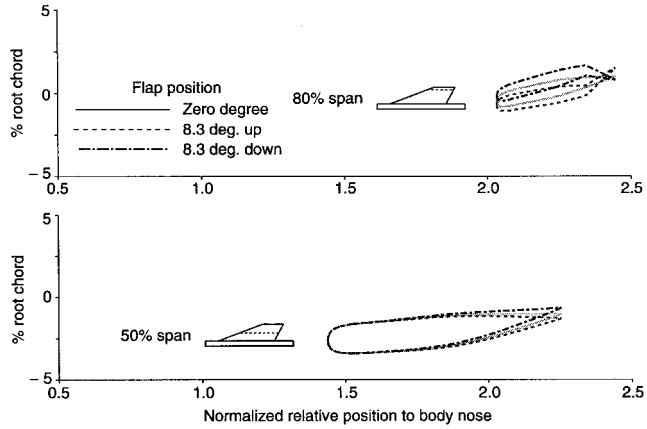

Fig. 10 Sectional variations of deflection with different flap positions for a flexible wing structure.

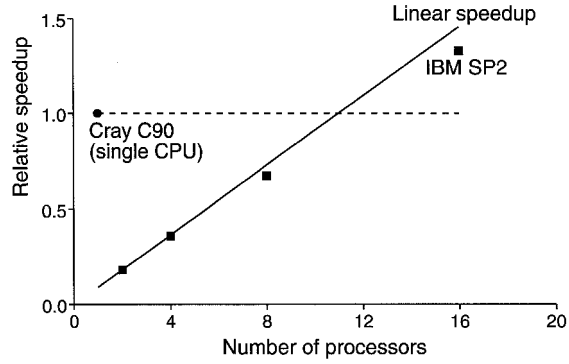

Fig. 11 Overall performance of multizonal version of ENSAERO for steady flow computations on the IBM SP2 computer.

machine. The half-span arrow wing–body configuration of 510,400 grid points is used for the performance measurement. By splitting and distributing the grid to various numbers of computational nodes, the wall-clock times are measured on the IBM SP2 computer. The zones are created by introducing appropriate zonal boundaries. The measurement on the SP2 is done for 2–16 computational nodes. The Cray time is obtained by solving the same configuration with two zones on a single processor of the Cray C90 computer. The relative speedup is obtained by comparing the wall-clock time on the SP2 with the CPU time obtained on a single processor of the Cray C90. As shown in Fig. 11, the speedup is quite close to linear speedup. Efficiency, the ratio of actual speedup with respect to linearly scaled speedup, is 91% when using 16 SP2 nodes. When using 12 computational nodes on the SP2, the performance of the parallel version of ENSAERO is equivalent to that obtained on a single processor of the Cray C90 computer.

Concluding Remarks

The parallel multizonal version of ENSAERO has been successfully implemented on the IBM SP2 computer. The multizonal capability for the fluid domain is extended to accommodate the aeroelastic computations for complex geometries. The implementation of the code on the SP2 is based on the domain decomposition method. Thus, each discipline is implemented on a separate group of computational processors.

For demonstration purposes, an arrow wing–body–control configuration is selected. The steady and unsteady flow simulations are carried out with and without flap deflections for both rigid and flexible wing configurations. The results show that significant changes in pressure distribution are a result of wing flexibility. The flexible structure reduced the sectional lifts significantly for the particular steady aeroelastic simulation. Further study should be made on the relation of structural

flexibility to dynamic aeroelastic responses coupled with controls for the transonic flow regime.

The performance obtained indicates that about 12 computational nodes of the SP2 computer are equivalent to the speed of a single C90 processor.

The multizonal aeroelastic capability in ENSAERO will enable the aeroelastic analysis of complex geometries. It can also be used for the fast computational solution of large-scale wind-tunnel models and real configurations that inevitably deform under aerodynamic loads.

Acknowledgments

This work was completed using the resources of the High Performance Computing and Communication Program (HPCCP) and Numerical Aerodynamic Simulation (NAS) Program at NASA Ames Research Center. The work done by the first author was funded through NASA Ames Research Center Fluid Dynamics Analysis Contract NAS2-14109.

References

[1]Guruswamy, G. P., "Navier-Stokes Computations on Swept-Tapered Wings, Including Flexibility," AIAA Paper 90-1152, April 1990.

[2]Obayashi, S., Guruswamy, G. P., and Goorjian, P. M., "Streamwise Upwind Algorithm for Computing Unsteady Transonic Flows Past Oscillating Wings," *AIAA Journal*, Vol. 29, No. 10, 1991, pp. 1668–1677; also Errata, *AIAA Journal*, Vol. 30, No. 2, 1992, p. 569.

[3]Obayashi, S., and Guruswamy, G. P., "Unsteady Shock-Vortex Interaction on a Flexible Delta Wing," *Journal of Aircraft*, Vol. 29, No. 5, 1992, pp. 790–798.

[4]Obayashi, S., and Guruswamy, G. P., "Navier-Stokes Computations for Oscillating Control Surfaces," AIAA Paper 92-4431, Aug. 1992.

[5]Obayashi, S., Chiu, I., and Guruswamy, G. P., "Navier-Stokes Computations on Full-Span Wing–Body Configuration with Oscillating Control Surfaces," AIAA Paper 93-3687, Aug. 1993.

[6]Flores, J., "Simulation of Transonic Viscous Wing and Wing-Fuselage Flows Using Zonal Methods," NASA TM-89421, March 1987.

[7]Byun, C., and Guruswamy, G. P., "Wing-Body Aeroelasticity Using Finite-Difference Fluid/Finite-Element Structural Equations on Parallel Computers," AIAA Paper 94-1487, April 1994.

[8]Fineberg, S., "MPIRUN: A Loader for Multidisciplinary and Multizonal MPI Applications," *NAS News*, Vol. 2, No. 6, 1994, pp. 1–6.

[9]"MPI: A Message-Passing Interface Standard," Message Passing Interface Forum, Univ. of Tennessee, Knoxville, TN, May 1994.

[10]Manro, M. E., Manning, K. J. R., Hallstaff, T. H., and Rogers, J. T., "Transonic Pressure Measurements and Comparison of Theory to Experiment for an Arrow-Wing Configuration," NASA CR-2610, Aug. 1976.

[11]Ruhlin, C. L., and Pratt-Barlow, C. R., "Transonic Flutter Study of a Wind-Tunnel Model of an Arrow-Wing Supersonic Transport," AIAA Paper 81-0654, April 1981.

[12]Baldwin, B. S., and Lomax, H., "Thin-Layer Approximation and Algebraic Model for Separated Turbulent Flows," AIAA Paper 78-257, Jan. 1978.

[13]Degani, D., and Schiff, L. B., "Computations of Turbulent Supersonic Flows Around Pointed Bodies Having Crossflow Separation," *Journal of Computational Physics*, Vol. 66, No. 1, 1986, pp. 173–196.

[14]Obayashi, S., and Guruswamy, G. P., "Convergence Acceleration of a Navier-Stokes Solver for Efficient Static Aeroelastic Computations," *AIAA Journal*, Vol. 33, No. 6, 1995, pp. 1134–1141.

[15]Bathe, K.-J., *Finite Element Procedures in Engineering Analysis*, Prentice–Hall, Englewood Cliffs, NJ, 1982.

[16]Byun, C., and Guruswamy, G. P., "A Comparative Study of Serial and Parallel Aeroelastic Computations of Wings," NASA TM-108805, Jan. 1994.

[17]"ICEM-CFD User's Guide Version 3.0," ICEM-CFD Engineering, Berkeley, CA, Aug. 1992.

[18]Chan, W. M., and Steger, J. L., "Enhancement of a Three Dimensional Hyperbolic Grid Generation Scheme," *Applied Mathematics and Computation*, Vol. 51, Oct. 1992, pp. 181–205.